AFRL-RY-WP-TR-2014-0045

PIEZOELECTRIC NON-LINEAR NANOMECHANICAL TEMPERATURE AND ACCELERATION INTENSIVE CLOCKS (PENNTAC)

Gianluca Piazza

Carnegie Mellon University

Kimberly Turner

University of California Santa Barbara

Brian Otis

University of Washington

Todd Palmer

Vectren International

Valeriy Felmetsger

OEM Group

MAY 2014
Final Report

AIR FORCE RESEARCH LABORATORY
SENSORS DIRECTORATE
WRIGHT-PATTERSON AIR FORCE BASE, OH 45433-7320
AIR FORCE MATERIEL COMMAND
UNITED STATES AIR FORCE

NOTICE AND SIGNATURE PAGE

Using Government drawings, specifications, or other data included in this document for any purpose other than Government procurement does not in any way obligate the U.S. Government. The fact that the Government formulated or supplied the drawings, specifications, or other data does not license the holder or any other person or corporation; or convey any rights or permission to manufacture, use, or sell any patented invention that may relate to them.

This report is the result of contracted fundamental research deemed exempt from public affairs security and policy review in accordance with SAF/AQR memorandum dated 10 Dec 08 and AFRL/CA policy clarification memorandum dated 16 Jan 09. This report is available to the general public, including foreign nationals.

AFRL-RY-WP-TR-2014-0045 HAS BEEN REVIEWED AND IS APPROVED FOR PUBLICATION IN ACCORDANCE WITH ASSIGNED DISTRIBUTION STATEMENT.

//SIGNED//

DONALD L. AGRESTA, Program Manager
Electro-Optic Components Branch
Aerospace Components & Subsystems Division

//SIGNED//

MARK G. SCHMITT, Chief
Electro-Optic Components Branch
Aerospace Components & Subsystems Division

//SIGNED//

BRADLEY D. CHRISTIANSEN, USAF, Lt. Col
Deputy Division Chief
Aerospace Components & Subsystems Division
Sensors Directorate

This report is published in the interest of scientific and technical information exchange, and its publication does not constitute the Government's approval or disapproval of its ideas or findings.

*Disseminated copies will show "//signature//" stamped or typed above the signature blocks.

REPORT DOCUMENTATION PAGE

Form Approved
OMB No. 0704-0188

1. REPORT DATE *(DD-MM-YY)*	2. REPORT TYPE	3. DATES COVERED *(From - To)*
May 2014	Final	20 August 2012 – 1 January 2014

4. TITLE AND SUBTITLE
PIEZOELECTRIC NON-LINEAR NANOMECHANICAL TEMPERATURE AND ACCELERATION INTENSIVE CLOCKS (PENNTAC)

5a. CONTRACT NUMBER
FA8650-12-1-7264

5b. GRANT NUMBER

5c. PROGRAM ELEMENT NUMBER
61101E

6. AUTHOR(S)
Gianluca Piazza (Carnegie Mellon University)
Kimberly Turner (University of California Santa Barbara)
Brian Otis (University of Washington)
Todd Palmer (Vectren International)
Valeriy Felmetsger (OEM Group)

5d. PROJECT NUMBER
1000

5e. TASK NUMBER
YD

5f. WORK UNIT NUMBER
Y0U2

7. PERFORMING ORGANIZATION NAME(S) AND ADDRESS(ES)
Carnegie Mellon University
Office of Sponsored Projects
5000 Forbes Avenue
Pittsburgh, PA 15213-3815
University of California Santa Barbara
University of Washington
Vectren International
OEM Group

8. PERFORMING ORGANIZATION REPORT NUMBER
AFRL-RY-WP-TR-2014-0045

9. SPONSORING/MONITORING AGENCY NAME(S) AND ADDRESS(ES)
Air Force Research Laboratory
Sensors Directorate
Wright-Patterson Air Force Base, OH
45433-7320
Air Force Materiel Command
United States Air Force
Defense Advanced Research Projects Agency DARPA/MTO
675 North Randolph Street
Arlington, VA 22203-2114

10. SPONSORING/MONITORING AGENCY ACRONYM(S)
AFRL/RYDP

11. SPONSORING/MONITORING AGENCY REPORT NUMBER(S)
AFRL-RY-WP-TR-2014-0045

12. DISTRIBUTION/AVAILABILITY STATEMENT
Approved for public release; distribution unlimited. This report is the result of contracted fundamental research deemed exempt from public affairs security and policy review in accordance with SAF/AQR memorandum dated 10 Dec 08 and AFRL/CA policy clarification memorandum dated 16 Jan 09.

13. SUPPLEMENTARY NOTES
Report contains color

14. ABSTRACT
During Phase II our team has tackled the main challenges related to the demonstration of low noise and high-frequency miniaturized aluminum nitride (AlN)-based frequency sources. Given the Phase I demonstration by our team, we have especially focused on understanding the noise sources in our oscillators and identifying new methods to evade phase noise.

15. SUBJECT TERMS
oscillators, aluminum nitride, low noise, high frequency

16. SECURITY CLASSIFICATION OF:			17. LIMITATION OF ABSTRACT:	18. NUMBER OF PAGES	19a. NAME OF RESPONSIBLE PERSON (Monitor)
a. REPORT	b. ABSTRACT	c. THIS PAGE			Donald Argesta
Unclassified	Unclassified	Unclassified	SAR	34	19b. TELEPHONE NUMBER *(Include Area Code)* N/A

Table of Contents

Section **Page**

List of Figures

Figure **Page**

Figure **Page**

1.0 Phase II Accomplishments

During Phase II our team has tackled the main challenges related to the demonstration of low noise and high-frequency miniaturized aluminum nitride (AlN)-based frequency sources. Given the Phase I demonstration by our team, we have especially focused on understanding the noise sources in our oscillators and identifying new methods to evade phase noise. Briefly, we summarize in bullet form the main accomplishments and contributions made in understanding and engineering miniaturized frequency sources. The following sections of this report provide more in depth details relative to each accomplishment.

1) We demonstrated the ability to use parametric bifurcation to filter and shape the noise of a 227-megahertz (MHz) AlN oscillator. ***The resulting phase noise (PN) at 1 kHz offset scaled to a 1-gigahertz (GHz) carrier is - 111 decibel/hertz (dBc/Hz)***. The obtained PN value exceeds the Phase II milestone. A general theory describing this phenomenon was also derived.
2) We identified major source of damping in high-frequency AlN contour-mode resonators. Anchor losses are dominant for frequencies in the range of 200-300 MHz, whereas interfacial dissipation (electode/AlN interface) dominates above 750 MHz. Segmented electrodes were introduced to reduce damping without affecting the resonator transduction efficiency.
3) We demonstrated the ability to use duffing non-linearities in AlN resonators to cancel amplifier phase noise below the thermal time constant of the resonator. Practical demonstration is described by theoretical model. This demonstration can be broadly applied to other non-linear resonators.
4) We identified frequency flicker noise in the AlN resonator as the main PN limiting mechanism when a low noise amplifier is used. A non-linear model describing the resonator noise was generated and imported into a standard circuit simulator.
5) Temperature compensation via resonator ovenization was experimentally demonstrated. Two methods of using ovenization were implemented and demonstrated. ***A final temperature stability of < 2 ppm from – 40 to + 85 °C was demonstrated for a microcontroller-based ovenized oscillator***. Fundamental limits associated with resonator aging and frequency variations were identified and will be considered in driving Phase III developments.
6) ***An acceleration sensitivity < 40 ppb/G was recorded for vibration frequencies between 100 Hz and 2 kilohertz (kHz)***. Acceleration sensitivity < 1 ppb/G was recorded for the higher vibration frequencies. We have identified the major sources of acceleration sensitivity to be in the component mounting and wirebonds.
7) ***The temperature and acceleration insensitive devices were demonstrated with components that occupy a total volume < 31 mm^3***. The majority of the volume is occupied by the discrete components used for the resonator ovenization circuit. Plans have been made to use integrated circuits for such a demonstration in Phase III.

2.0 Parametric Bifurcation Enables Phase Noise Filtering

We excite parametric bifurcation in a parametric divider formed by a non-linear varactor and two parallel tanks set a ω_0 and $2\omega_0$, ω_0 being the oscillator carrier frequency (Fig. 1). The parametric divider is placed at the output of the AlN resonator based oscillator. The oscillator output frequency is first doubled and its magnitude amplified prior to feeding the parametric divider. A second loop taking the output of the parametric divider and feeding the signal back to the amplifier is also introduced to reduce the amplifier direct current (DC)-power needed to activate the division. A parametric divider is a 2-port network that transfers energy from an input signal at ω to an output signal at $\omega/2$. Above a certain input power a system pole becomes unstable and a flip-type bifurcation occurs. The unstable pole causes the rising of a sub-harmonic oscillation. This activation power is mostly set by the varactor DC-bias, V_{dc}, and by the input power, $P_{in}(2\omega_0)$.

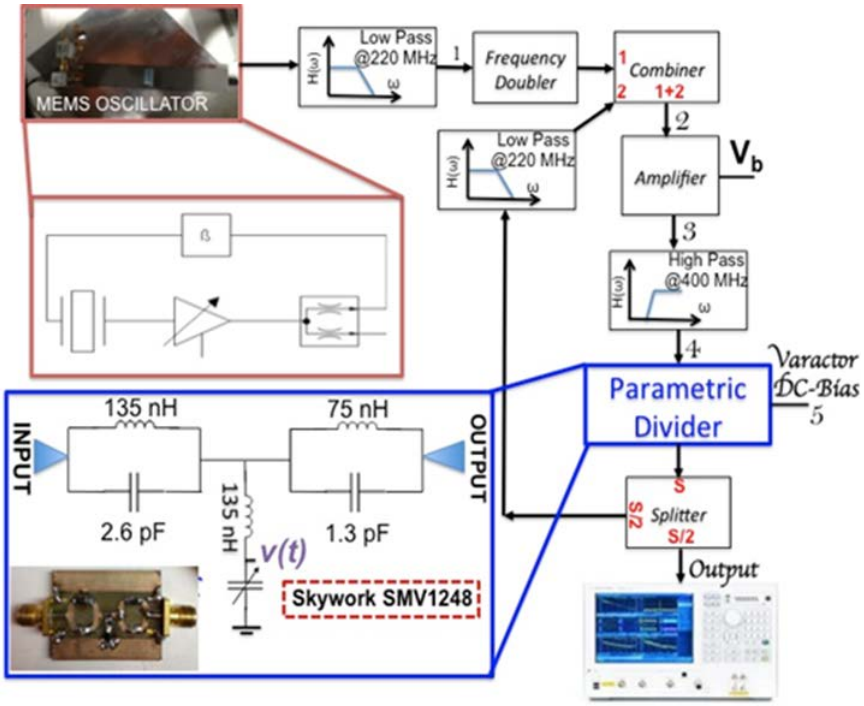

Figure 1: Parametric Filtering Topology used to reduce Oscillator PN

The output at ω_0 of the feedback-loop oscillator, based on a 227 MHz AlN resonator, is filtered around the oscillation frequency and sent to a frequency doubler (1). The output of the frequency doubler is amplified (2), filtered (3) and sent to the parametric divider input (4). The varactor DC-bias, V_{dc}, and the divider input power, P_{in}, regulated by the amplifier bias voltage, V_b, sets the divider working point. Half of the divider output is sent to the output load. The other half is sent back to the input of the amplifier (2) to reduce the amplifier DC-power consumption.

Considering the parametric circuit (Fig. 1), and using the voltage across the varactor, $v(t)$, as the only state variable, it is possible to define a complex admittance $Y_T(\omega_0)$, function of $P_{in}(2\omega_0)$ and V_{dc}:

$$Y_T(\omega_0) = Y_T(P_{in}(2\omega_0), 2\omega_0, V_{dc}) \quad (1)$$

Under the assumption that $Y_T(\omega_0)$ is real close to the division threshold, and no white noise is added by the divider circuit, the spectrum of the PN of the sub-harmonic oscillation, $\Delta\varphi_T(\Omega)$, where Ω is the frequency offset is given by:

$$|\Delta\varphi_T(\Omega)|^2 = \frac{[\frac{dY_T}{d\varphi}]^2 \cdot [\varphi_s(\Omega)/2]^2}{[\frac{dY_T}{d\varphi}]^2 + [\frac{dY_T}{d\omega}]^2 \cdot \Omega^2} \quad (2)$$

Eq. (2) shows that for small Ω the PN of the divider tends to the linear prediction (ϕs(Ω)/2). For larger Ω (> 10-100 Hz) and especially for a large derivative of the admittance with respect to frequency, the second term at the denominator plays a key role. By regulating the varactor DC-bias it is possible to modify the divider working point and make it operate close to the bifurcation region, where $dY_T/d\omega$ is maximized. Effectively, this phenomenon enables reduction of the oscillator PN because the divider is not able to track the fast noise perturbations of the micro-electrical mechanical system (MEMS) oscillator. In the case of a 227 MHz AlN oscillator, this technique brought > 26 dB improvement in the PN at Ω =10 kHz offset and > 20 dB improvement at Ω =1 kHz offset (Fig. 2-3). This technique yields a PN of – 124 dBc/Hz at 1 kHz offset for a 227 MHz carrier. Referenced to a 1 GHz carrier, this PN corresponds to - 111 dBc/Hz. To our knowledge this is the lowest PN ever reported for any MEMS based oscillator. The demonstrated technique is of general value and could be applied to any MEMS oscillator. In the appendix we provide a generalized description of noise filtering that occurs in a parametric system starting from the Mathieu's equation. This description solidifies our experimental demonstration from a theoretical standpoint and offer further guidance in the design of a higher frequency oscillator in phase III.

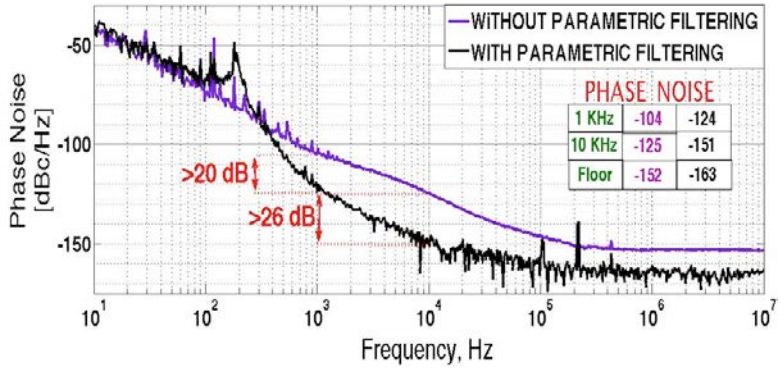

Figure 2: In purple: PN for the Feedback Loop 227 MHz Oscillator without Parametric Filtering. In black: PN at the Output of the Parametric Filter when V_{dc} is 2.07 V and V_b=16V.
In this case the system is working close to the division bifurcation.

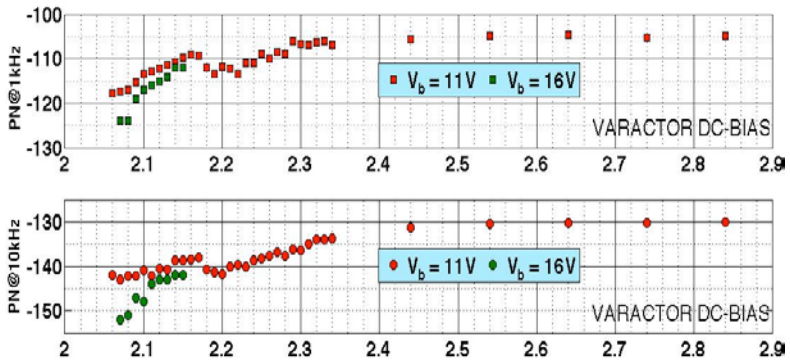

Figure 3: Squares: PN at 1 kHz offset for different Varactor DC-biases and for Two Distinct Amplifier Bias Voltages, V_b (Fig. 1). Circles: PN at 10 kHz offset for different Reverse Varactor DC-biases and for Two Distinct Amplifier Bias Voltages, V_b (Fig. 1).

In the case in which V_b=16V, the sub-harmonic oscillation occurs for a much narrower range of varactor DC-biases (2.07 - 2.15 V). When no parametric filtering is used the phase noise is - 104 dBc/Hz at 1 kHz offset and -125 dBc/Hz at 10 kHz offset. Instead, the use of parametric filtering enables 20 dB improvement in the phase noise at Ω=1 kHz and 26 dB at Ω=10 kHz.

3.0 Mitigation of Anchor Losses and Interfacial Dissipation in AlN Contour-Mode Resonators

Although we do not target improving the resonator Q to reduce the oscillator phase noise (an approach that we will prove of little effectiveness in the section on resonator flicker noise), it is important to understand the sources of damping in our resonator to ensure that Q > 1,000 are available at high frequencies. This is essential in justifying the use of an acoustic resonator over lumped components (LC) in conjunction of parametric filtering, as it will yield an overall lower phase noise source.

To this purpose we have systematically studied the behavior of 324 devices having a fixed AlN plate size (60x144 µm), operating at 3 different frequencies (220, 370 and 1050 MHz), and having variable anchor size (function of the acoustic wavelength, λ). Each particular condition was tested in 9 separate devices so that meaningful statistics could be collected. The experimental results are shown in Fig. 4. It is evident that anchor losses (energy escaping through the resonator supports) play a dominant role at frequencies in the range of 200-300 MHz. At higher frequencies, the resonator damping is instead dominated by interfacial dissipation (due to a stress jump occurring at the interface between the AlN film and the electrodes). To mitigate both sources of damping in the resonators we have included etched air slots at the anchor location (Fig. 5-left) or introduced segmented electrodes to reduce the electrode area coverage without impacting the device electromechanical coupling (Fig. 5-right). These two approaches have yielded respectively a 50 % improvement in Q at 220 MHz (etched slots) and at 750 MHz (segmented electrodes).

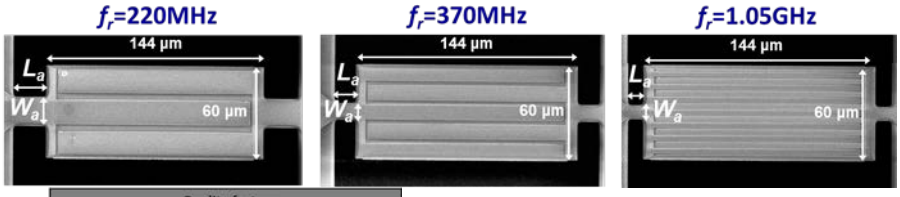

		Quality factor					
		fs=220MHz		fs=370MHz		fs=1.05GHz	
Wa/λ	La/λ	Avg	Stand Dev	Avg	Stand Dev	Avg	Stand Dev
1/4	1/4	1532	448	1424	500		
1/2	1/4	2343	1014	1468	694	1331	510
1	1/4	520	150	667	267	1586	357
3/2	1/4	932	212	1116	386	1606	530
1/4	1/2	1356	414	1112	480		
1/2	1/2	2180	1184	1350	570	1183	460
1	1/2	718	249	841	302	1219	668
3/2	1/2	1201	336	1124	460	1634	453
1/4	1	1191	322	1183	392		
1/2	1	2318	938	1387	507	1189	465
1	1	773	206	1055	300	1496	491
3/2	1	1325	244	1132	408	1657	418

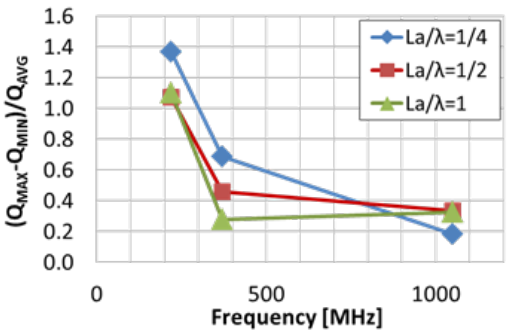

Figure 4: (Top) Basic Resonator Geometry and Parametric Variations for different Frequencies. (Bottom-left) Table showing average Q and Standard Deviation (9 samples each) for Resonators of different Anchors Width, Wa, and Length, La. (Bottom-right) Plot showing how Q varies largely as a Function of Anchor Size at lower Frequencies.

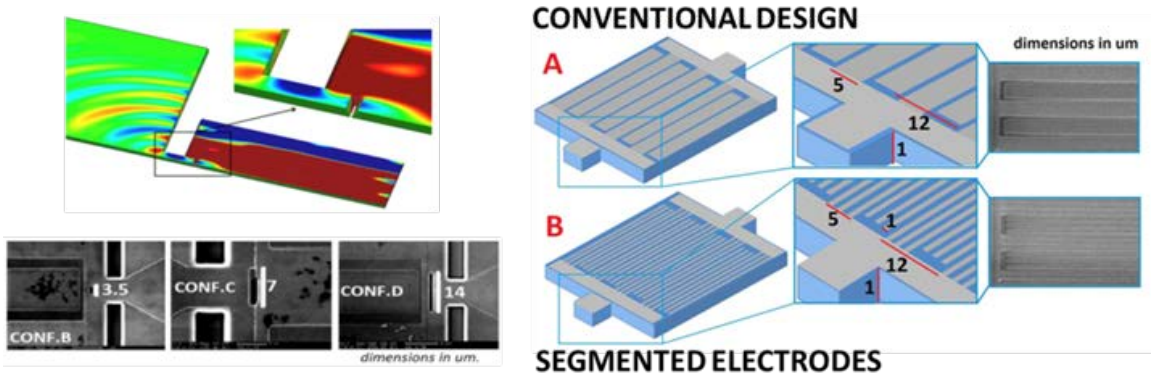

Figure 5: (left) Example of different Types of Slots that were introduced in the Resonator Body near the Anchor in order to minimize the Amount of Energy Escaping through the Supports. (right) Comparison between a Conventional Resonator Design and a segmented Electrode One.
The segmented electrode design reduces the electrode area coverage without altering the resonator electromechanical coupling.

3.1 Duffing Resonator Cancels Amplifier Noise

In phase I we have shown that the resonator self-heating is the leading source of a softening nonlinear behavior in our AlN contour mode resonators. We illustrated that the measured resonator admittance exhibits a softening behavior, but that the amount of bending in the resonance depends on the rate of frequency sweep employed in the measurement. We further showed that self-heating in our AlN resonators can be described with a Duffing resonator model. However, this analysis was performed in the quasi-static limit. In this phase, we considered the complete dynamic model of a self-heating AlN resonator and analyzed the response of the resonator to a frequency sweep through resonance and its relationship to the sweep rate. In addition, we illustrated that while the self-heating nonlinearity appears similar to the Duffing nonlinearity in the quasi-static case, its dynamics are different. This has important implications, especially related to the ability of these resonators to evade amplifier noise in oscillators using the techniques described by Yurke, *et al.*

We introduced a non-liner resonator model (Fig. 6), which describes the first order dependence of the mechanical (motional) components (R_m, L_m, C_m) on temperature. The resonator is described by the following set of differential equations:

$$
\begin{aligned}
L_m \ddot{q}_m + (R_m + R_s)\,\dot{q}_m + \frac{1}{C_m} q_m &= V - R_s \dot{q}_0, \\
(R_0 + R_s)\dot{q}_0 + \frac{1}{C_0} q_0 &= V - R_s \dot{q}_m, \\
C_{\text{th}} \dot{T} + \frac{T}{R_{\text{th}}} &\approx (R_m^{(0)} + R_s)\dot{q}_m^2.
\end{aligned}
\tag{3}
$$

where

$$
\begin{aligned}
L_m &\approx L_m^{(0)} + L_m^{(1)} T, \\
R_m &\approx R_m^{(0)} + R_m^{(1)} T, \\
C_m &\approx C_m^{(0)} + C_m^{(1)} T.
\end{aligned}
$$

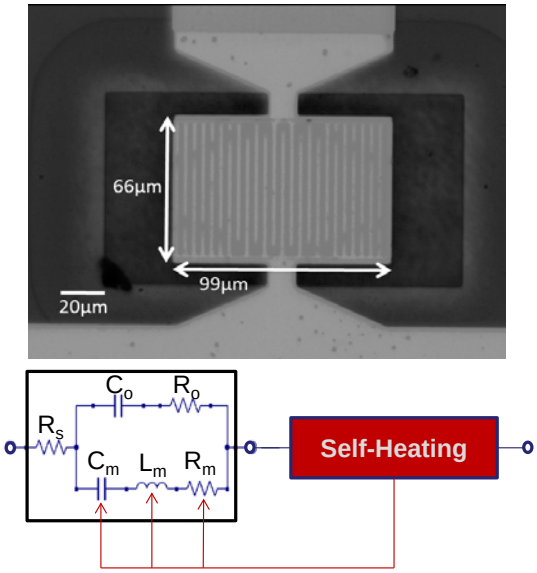

Figure 6: (Top) Microscope Image of a 1 GHz AlN Contour-mode Resonator (Bottom) Modified Butterworth Van Dyke (MBVD) Circuit Model with Nonlinear Motional Elements

By solving this set of equations, we were able to accurately predict the resonator response when excited by an external network analyzer for different signal sweep rates (Fig. 7). These results imply that we can correctly picture the resonator dynamics and use the aforementioned model in a closed-loop oscillator to predict phase noise shaping in the presence of strong non-linearities.

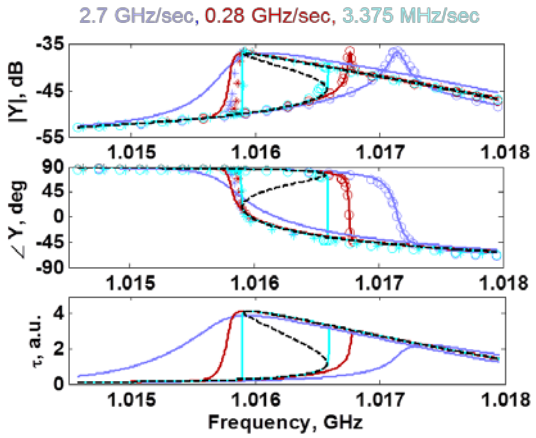

Figure 7: Experimental (Discrete Points) and Fitted (Continuous Line) Response
From top to bottom: admittance magnitude, admittance phase, and resonator temperature) of a 1 GHz AlN contour-mode resonators for different input signal sweep rates. The input power was kept constant at 11 dBm. It is evident that the resonator behavior depends on the sweep rate, a clear sign that its dynamics are regulated by the device thermal time constant. The overlaid dashed black line represents the fixed point solution of the Duffing resonator.

Resonator non-linearities tend to worsen the oscillator PN by converting amplitude noise to frequency noise. Nonetheless, this non-linear phenomenon can also be exploited for evading amplifier phase fluctuations as previously shown by Yurke, *et al.* In fact, a non-linear resonator exhibits specific phase/frequency relationship for which the oscillator dynamics can be substantially modified. Intuitively, the resonator time constant can be made infinite at special operating points generated by the resonator non-linearity. When the resonator is locked in that particular state in a closed-loop oscillator, then the amplifier phase fluctuations can be eliminated. To prove this theory we have built a 222 MHz oscillator using coaxial electronic components (Fig. 8-top). In this case, the AlN contour-mode resonator (CMR) is mounted on a 2-port printed circuit board (PCB) (Fig. 8-bottom) that is connected in series with the rest of the components in the circuit. All the discrete elements, subminiature version A (SMA) connectors, and cables are chosen to have the characteristic impedance equal to 50 Ω for matching purposes. An external DC power supply is used to bias the radio frequency (RF) amplifier (Mini-circuits ZKL-1R5+) and the output is taken from one of the power divider (M/A-COM T-1000) terminals. To close the loop, one terminal is connected to the phase shifter (ATM P1213). In this particular implementation, the selected amplifier was characterized by a large intrinsic $1/f^2$ noise. When driving the resonator non-linearly (by means of sufficient gain) and tuning the loop phase, it was possible to identify specific working points that yielded a significant phase noise reduction (Fig. 9). The PN reduction was limited to frequency offsets below the resonator thermal time constant. The obtained results can be fit by theoretical predictions. It is important to note that PN cancellation occurs only for noise sources external to the resonator. When the noise source is intrinsic to the resonator (see next section) this technique is not applicable. Nonetheless, the practical demonstration is of general interest in proving the use of non-linearity for shaping phase noise. Our team has ultimately used a different approach based on parametric filtering to meet the stringent phase noise requirements dictated by the DARPA program. For this reason, this approach will be considered during phase III, if and only if, ways to mitigate the resonator flicker noise will be identified.

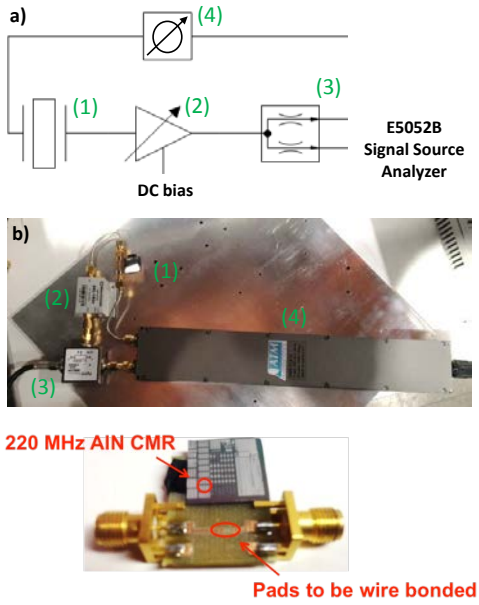

Figure 8: (Top) Schematic and Actual implementation of the Oscillator Setup used to demonstrate PN shaping via a Duffing Resonator. (1) AlN CMR mounted on a PCB, (2) RF Amplifier, (3) Power Divider, and (4) Phase Shifter. (Bottom) Photograph of 222MHz AlN CMR Wire Bonded on a 2 port FR4 Circuit Board.

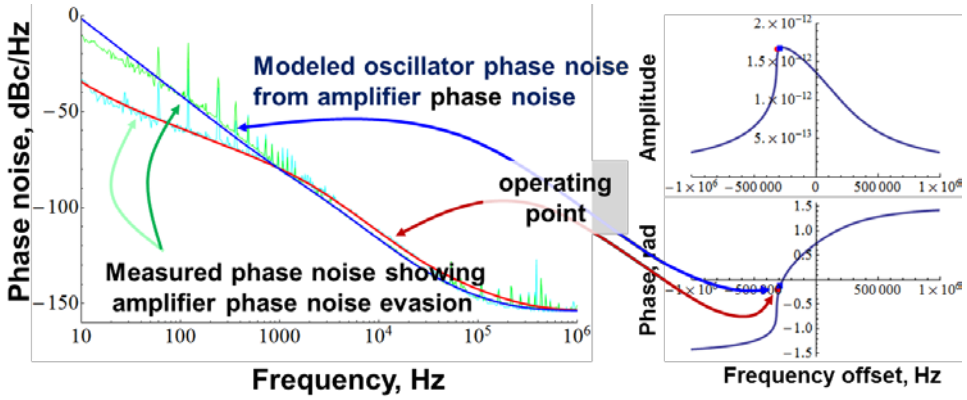

Figure 9: Measured Phase Noise Response of the Non-linear 222 MHz AlN Oscillator for different Phase Conditions (green and light blue curves)

The predicted PN response is overlapped (blue and red curves). It is clear that the oscillator PN is reduced for particular amplitude and phase conditions exhibited by the Duffing resonator

3.2 1/f Resonator Flicker Noise

In order to identify the main noise sources in our oscillators, and especially explain the origin (whether due to mechanical or electronic components) of the $1/f^3$ slope generally seen in the phase noise plots,

we have separately measured the amplifier baseband noise and the resonator frequency fluctuations. The measurement of the latter was complicated by the lack of sensitive equipment. Ultimately, we were able to develop a method to measure resonator frequency fluctuations with a network analyzer. In a simplified way the method is based on observing the phase fluctuations in the reflection coefficient (or transmission coefficient) of a resonator excited by a fixed frequency signal. As long as the resonator exhibits a noise greater than the signal source, it is possible to extract the resonator frequency fluctuations. We have measured 128 different devices, operating at different frequencies, having varying AlN film thickness and electrode materials, and fabricated at different facilities (University of Pennsylvania, Carnegie Mellon University, Sandia National Laboratories (SNL) and the Institute of Microelectronics (IME) in Singapore). Interestingly, as shown in Fig. 10, there is no dependence of noise on device Q, volume or frequency of operation (note that the equivalent closed-loop noise at 1 Hz offset is referenced to a 1 GHz carrier). It appears that the use of Pt electrodes reduces the resonator frequency fluctuations. Also a common feature for the devices fabricated at SNL and IME was the use of an oxide film to isolate the resonator from the high resistivity silicon wafer. Although no conclusive statement can be made at this stage on the physical source of frequency fluctuations in the resonators, we can confidently state that the oscillator close-in phase noise is limited by the acoustic device and not the electronics. Fig. 11 is a clear evidence of this conclusion. The same trend was also seen in various other oscillators.

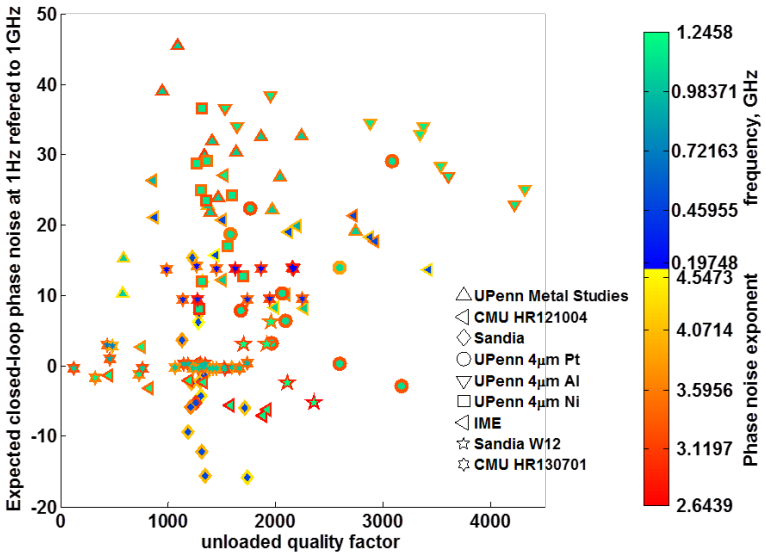

Figure 10: Plot of the expected Closed-loop Phase Noise at 1 Hz offset referenced to 1 GHz Carrier for 128 different Devices vs. Measured Device Q

The inner color of each symbol corresponds to the frequency of operation indicated on the scale bar. The outer color of each symbol refers to the exponent, n, of the phase noise ($1/f^n$).

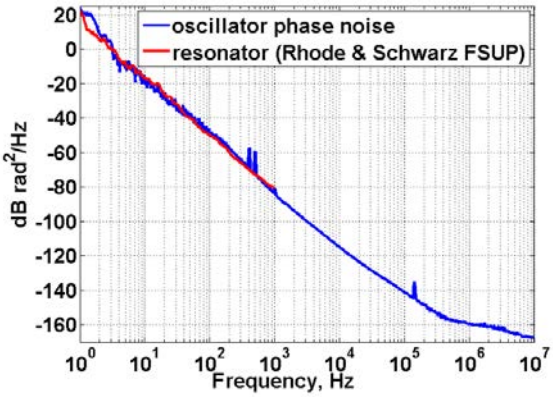

Figure 11: Comparison of measured 1 GHz Oscillator Phase Noise and expected Closed-loop Oscillator Phase Noise based on Open Loop Measurement of Resonator frequency Fluctuations

The open loop measurement was performed with both the network analyzer and the Rhode & Schwarz FSUP. The two instruments give the same expected noise, but the Rhode & Schwarz FSUP has a higher measurement bandwidth (up to 1 kHz).

We have also formalized these conclusions by generating an equivalent circuit model in advanced design system (ADS). The model (Fig. 12-left) describes the resonator non-linearity, its frequency flicker noise, and the amplifier (in this case a SiGe BJT) flicker noise. The model can be used to accurately predict the closed-loop behavior of the oscillator phase noise (Fig. 12-right). The development of such electronic model is a key step forward in the design of high performance MEMS oscillators and will have a broader impact on the device and circuit communities.

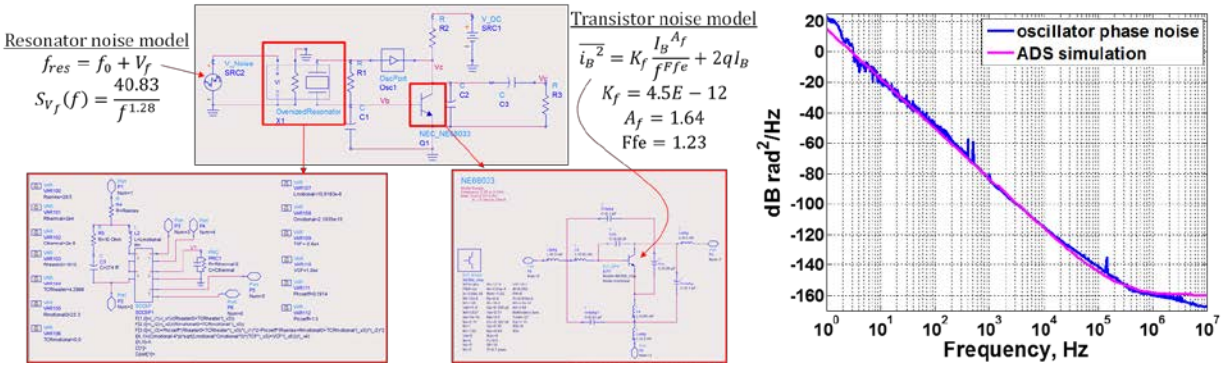

Figure 12: (Left) ADS Oscillator Circuit Model incorporating AlN CMR Non-linearity, Resonator frequency Flicker Noise, and Amplifier Flicker Noise (Right) Measured PN response of 1 GHz Oscillator compared to prediction made through ADS Model

Note that no fitting parameters are used, but noise sources are directly measured in open loop. The overlap between simulation and experiments confirm the validity of the developed model.

3.3 Temperature Compensation

In Phase II we used the same temperature compensation approach we developed in Phase I, but added the ability of using a microntroller to fine tune the oscillator temperature stability and meet Phase II metrics. The compensation technique is based on integrating a resistive heater with the resonator to either ovenize the device or tune its center frequency in response to temperature changes. As shown in Fig. 13, we looked at 3 different ways of integrating the heater with the resonator: (a) under the body of the resonator, (b) on the top surface around the perimeter of the resonator; (c) suspended above the resonator body. The rationale beyond moving the heater outside the resonant body was to limit its impact on the acoustic performance of the resonator. This is done at the expenses of increasing the power dissipated to elevate the resonator temperature because a greater thermal resistance path exists between the heater and the device. Ovenized oscillators were built using all 3 different heater implementations.

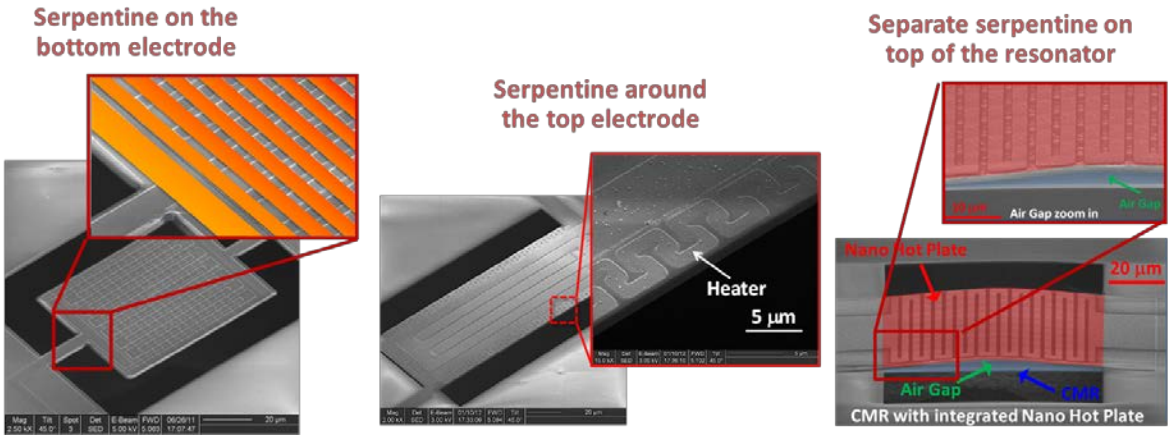

Figure 13: Three different ways of integrating a Serpentine Heater with the AlN Resonator
(Left to right) heater on the bottom electrode, heater around the device perimeter of the resonator, heater suspended on top of the resonator

As in phase I, the use of a Wheatstone bridge to control the ovenized oscillator showed a temperature dependence of about 130-160 ppm over - 40 to + 85 °C. In Phase II, attention was placed in selecting resistive components that form the Wheatstone bridge with very low temperature coefficient of resistance. Nonetheless, it appears that the temperature stability of the ovenized oscillator is limited by the sustaining amplifier. A major improvement from phase I was to use an integrating circuit instead of a proportional controller to stabilize the resonator temperature (Fig. 14). Such technique enabled us to keep a more stable resonator frequency over time.

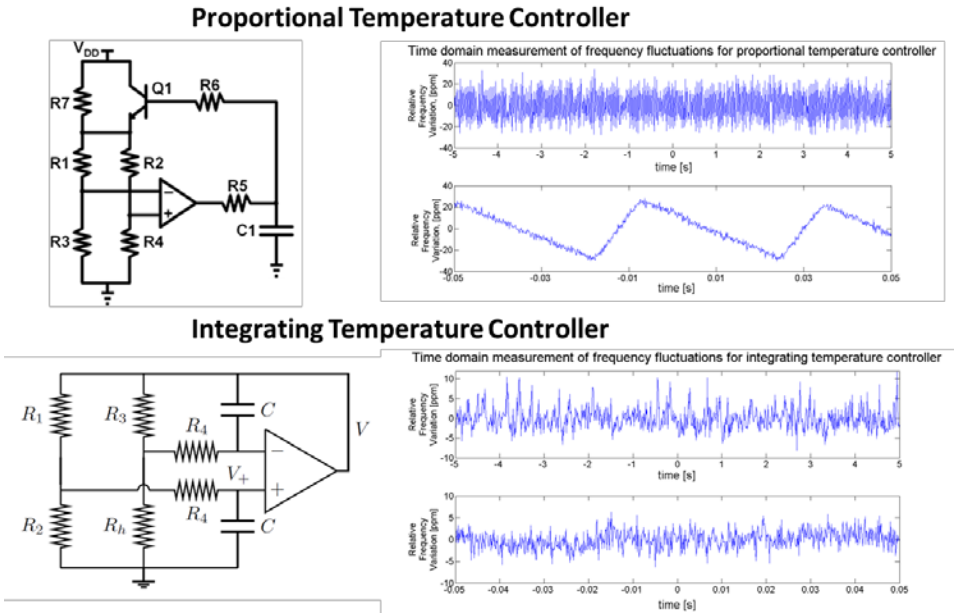

Figure 14: Comparison of Two Ovenization Techniques to achieve Temperature Compensation
(Top) proportional circuit used in Phase I based on a wheatstone bridge, an amplifier and a switch (BJT) to control the resonator temperature. Although an overall stability of about 130 ppm was attained, the temperature fluctuates by ~ ±20 ppm over time. (Bottom) integrating circuit implemented in Phase II and based on the same wheatstone bridge, but with a simple amplifier and RC network in the feedback loop. Similar overall temperature stability was attained, but this circuit results in a much tighter control of frequency over time with fluctuations < ± 5 ppm.

A second approach that uses the heater as a mechanism to pull the resonator frequency enabled us to meet the program requirements (Fig. 15). Frequency stability over temperature of 2 ppm was achieved. In this case, the resonator center frequency is programmed to be at a particular frequency at a given temperature by storing in the microcontroller the amount of current that needs to flow in the resonator. This method is agnostic of the source of frequency drift (whether the resonator or the circuit), hence it does not suffer from the issues of the Wheatstone bridge ovenized oscillators previously presented. This method, though, clearly requires a calibration process that measures few points on the oscillator frequency-temperature curve. For temperature values in between the measured ones an interpolation algorithm is used. Given the use of unpackaged devices and the aging of the resonator, the microcontroller needs to be programmed prior to any testing.

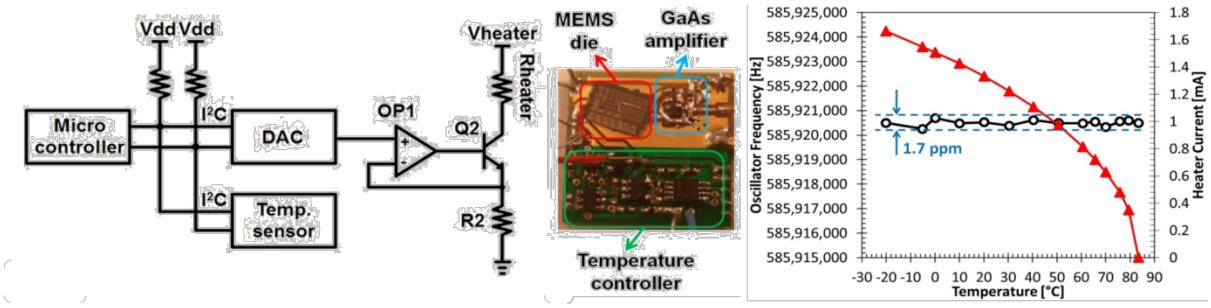

Figure 15: Microcontroller based Temperature Compensation Circuit

An external digital temperature sensor is used to monitor the environment temperature. The microcontroller is first calibrated and stores the amount of current that needs to be flown in the heater as a function of the external temperature. A practical implementation is shown in the middle of the figure. A GaAs amplifier is used to drive the MEMS resonator. The temperature controller is mounted on the same PCB and occupies a large fraction of the overall volume. A temperature stability of 1.7 ppm was obtained over the temperature range of – 25 to + 85 °C. A max current of 1.7 mA was used with a heater supply voltage equal to 12 V. The oscillator was not tested below – 25 °C to avoid electromigration in the Al heater. This issue is addressed by using a Pt heater.

Ultimately, we believe that an approach based on the resonator ovenization is simpler and will yield a more easily field-deployable component. For this reason, we have focused on finding ways to compensate for circuit temperature sensitivity. By properly designing the bias currents that feed the sustaining amplifier, we were able to minimize variations of the circuit operating point with temperature (Fig. 16). We strongly believe that this approach in conjunction with the use of integrated circuits will enable us to meet Phase III temperature compensation metrics in a very small form factor.

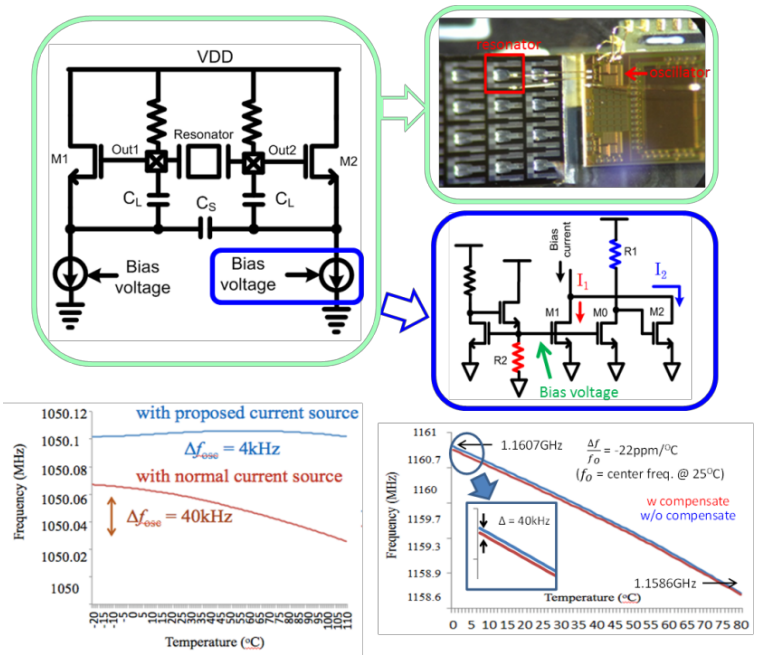

Figure 16: Temperature Insensitive Oscillator Circuit

By properly setting the direction and magnitude of the current flowing in the bias circuit over temperature it is possible to make the amplifier set point independent of temperature. This concept was proven experimentally with an uncompensated resonator. The circuit temperature sensitivity went from 40 ppm to 4 ppm.

3.4 Acceleration Sensitivity

Limited work was done in engineering the device acceleration sensitivity. The measurement of the acceleration sensitivity (Fig. 17) clearly highlights its dependence on factors other than the intrinsic resonator out-of-plane displacement. The oscillator Γ is well below the phase II metric (< 30 ppb/G for all vibration frequencies), but shows a linear dependence on the vibration frequency, which is likely indicative of poorly mounted components or wirebond vibrations. If we consider the vibration frequency of 2 kHz, we can see how our existing oscillator already meets phase III specifications. We plan to package and solder our components with a more permanent fixture so as to extract the ultimate device limit. In fact, COMSOL simulations predict that the device itself should have an acceleration sensitivity below 0.05 ppb/G.

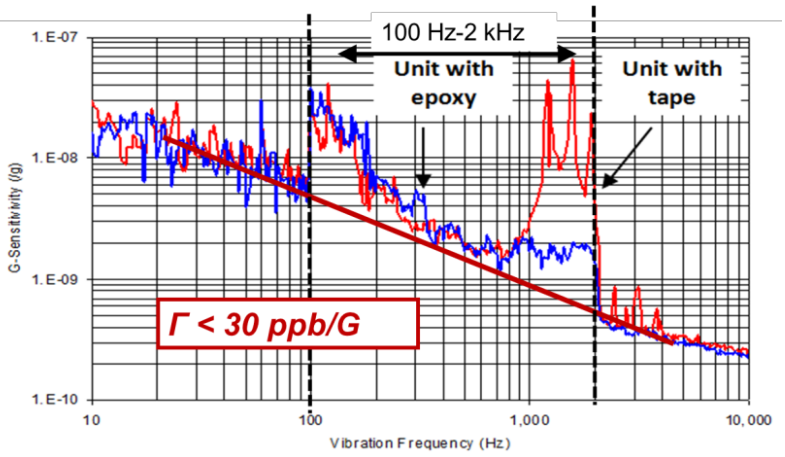

Figure 17: Acceleration Sensitivity Testing performed at Vectron on a Temperature Compensated Unit
The acceleration sensitivity is < 30 ppb/G for all vibration frequencies. It is clear that component mounting plays a key role as just epoxying some of the components reduces spurious peaks in the sensitivity plot.

3.5 Volume

Phase II metrics were met by using discrete components. Fig. 18 shows the overall volume taken by the components mounted on the PCB. It is clear that the greater part of the volume is consumed by the temperature controller. For this reason, we have started an effort on using integrated circuit (IC) for the implementation of the temperature controller. This controller will be synthesized and tested in Phase III.

Oscillator Circuit				
Component	**Area [mm²]**	**Thick. [mm]**	**Quantity**	**Volume [mm³]**
Transistor	1.68	0.7	1	1.18
Resistor	0.5	0.5	3	0.75
Capacitor	0.5	0.5	4	1
Resonator	0.25	0.5	1	0.13
Total Volume Oscillator Circuit				**3.05**
Temperature Controller				
Resistor	0.5	0.5	3	0.75
Capacitor	0.5	0.5	3	0.75
PIC12F1840	9	0.9	1	8.1
Temp sensor	5.94	0.9	1	5.35
DAC	5.94	0.9	1	5.35
Op. Amp	3.24	0.8	1	2.59
BJT	5.94	0.9	1	5.35
Total Volume Temperature Controller				**28.2**
OVERALL VOLUME				**31.25**

Figure 18: Volume of Discrete Components used for the Synthesis of the Ovenized Oscillator

3.6 Phase II Metric and Comparison with PENNTAC Team Accomplishments

	Frequency [MHz]	Phase Noise at 1 GHz for 1 kHz offset [dBc/Hz]	Acceleration Sensitivity [ppb/G]	Temperature Coefficient [ppm]	Volume [mm^3]
PHASE II METRIC	**800**	**- 110**	**100**	**10**	**30**
PENNTAC TEAM ACCOMPLISHMENTS	**> 800**	**- 111**	**< 40**	**2**	**31**

4.0 PHASE III PLANS

Phase III goals are listed below:

	Frequency [MHz]	Phase Noise at 1 GHz for 1 kHz offset [dBc/Hz]	Acceleration Sensitivity [ppb/G]	Temperature Coefficient [ppm]	Volume [mm^3]
PHASE II METRIC	**1000**	**- 120**	**10**	**3**	**1**

Briefly, in the following sections we outline our approach and risk mitigation for each metric. In summary, we will try to further lower the oscillator PN by using the parametric filtering technique identified in Phase II. Efforts will be placed in miniaturizing the components by using ICs so as to meet the stringent volume requirements. Low noise mechanical and electronic methods to perform parametric filtering will be identified. Simultaneously, we will explore techniques to mitigate the resonator intrinsic noise by investigating its fundamental physics and synthesizing coupled arrays. Finally, we will identify methods to further reduce its temperature sensitivity.

4.1 Frequency

This is a low risk goal for our team. We have already demonstrated resonator and oscillators operating up to 1 GHz. We can control the resonator geometry and fabrication to produce AlN resonators operating at 1 GHz. We are also familiar with the required electronics to design the electronic oscillator at this frequency. A greater challenge is posed by scaling and miniaturizing the electronics required to implement the parametric filter required to meet the Phase III metrics. To this purpose, we have decided to take an approach based on the design and implementation of these components using ICs.

4.2 Phase Noise

This is the highest risk metric for our team. Although we have identified a pathway that simultaneously will ensure us to attain low phase noise and miniaturization, we need to substantially improve the oscillator phase noise by another 10 dB. We plan to do so by: 1) continuing to study the fundamental noise sources in the resonator (which limits the noise in the sustaining oscillator) to identify the physical origin of the noise and methods to suppress it; 2) identifying solid-state or mechanical components capable of providing parametric noise filtering and characterized by a substantially lower intrinsic noise than off-the-shelf components; 3) using coupled resonant systems or arrays of resonators to cancel the resonator intrinsic flicker noise (Fig. 19).

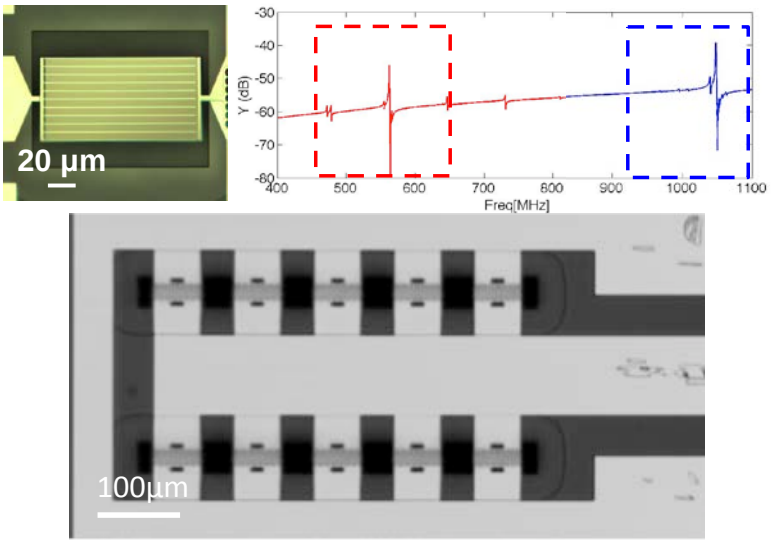

Figure 19: Examples of (top) Dual Mode Resonator and (bottom) Resonator Array that will be explored in Phase III to reduce the Oscillator Phase Noise

Addressing the issue of the noise source in the resonator is also essential in enabling other non-linear techniques that can only cancel noise sources external to the resonator. We believe that suppressing the resonator intrinsic noise could enable our team to apply other noise cancelling techniques, hence resulting in new significant gains in PN shaping. In phase II we have developed a basic theory that shows that the use of multiple synchronized references can be exploited to cancel the intrinsic noise in resonators (see Q3-2013 report). We plan to implement that theory in Phase III.

4.3 Acceleration Sensitivity

This is a low risk metric for our team, although the results of Phase II will need to be improved in order to meet the final goal. Our plan is to identify the major sources of low frequency vibrations and more appropriately package our devices. As we strongly believe that our oscillators are limited by external components, we are confident that the proposed approaches will be enough to ensure attaining an acceleration sensitivity < 1 ppb/G.

4.4 Temperature Coefficient

This metric is a medium risk task for our team. We believe that the approach used in Phase II can be scaled to Phase III. Although we have shown that temperature stability of about 2 ppm can be achieved, the approach is limited in its applicability as it requires a very stable device with low aging and drift. Resonator aging and drift directly impacts the repeatability of the measurements and limits the maximum stability that can be attained. We plan to study the resonator aging over time in order to bound the maximum stability that can be achieved. To this purpose we will use Vectron packaging capabilities and study our resonator behavior over periods of weeks. We will also investigate the physical reasons of aging and identify methods to mitigate it. In order to ensure more stable ovenized

resonators we also plan to introduce compensation layers in the structure of the resonator so as to start from a device with a lower intrinsic temperature coefficient of frequency (TCF).

Finally, we plan to implement an IC version of the temperature controller in addition to a temperature stable gain element to meet the volume requirements of Phase III. To this effect, efforts were already made in Phase II.

We will also investigate the oscillator start-up time according to MIL-PRF-55310E.

4.5 Volume

Phase II oscillator volume was limited by the size of the temperature controller. In order to meet the phase III metric we plan to focus on the miniaturization of the temperature controller. To this purpose, we plan to place the sustaining oscillator and the temperature controller on the same chip made with integrated circuits. The proposed approach will result in an overall volume of 1.12 mm^3 (see Fig. 20).

Temperature Compensated Oscillator				
Component	**Area [mm^2]**	**Thick. [mm]**	**Quantity**	**Volume [mm^3]**
Resonator	0.5	0.25	1	0.125
Oscillator + TDC and DAC	4	0.25	1	1
Total Volume				**1.125**

Figure 20: Expected Oscillator Volume in Phase III
The miniaturization of the temperature controller will reduce the overall volume to 1.125 mm^3.

5.0 APPENDIX

The Mathieu Resonator Model of Dynamic Phase Noise Filtering

A simple model exhibiting the phenomenon of dynamic phase noise filtering is the Mathieu resonator (our parametric divider),

$$\begin{aligned}\ddot{q} + 2\Gamma\dot{q} + (\omega_0^2 + 2\omega_0\xi(t) + 4\delta\Gamma\Omega\cos(2\Omega t + 2\theta(t) + \psi))q \\ = V_0\cos\big(\Omega t + \theta(t)\big) + n(t),\end{aligned} \tag{A1}$$

where $\xi(t)$ is an intrinsic fluctuation in the resonant frequency of the resonator, $n(t)$ is an additive white noise with autocorrelation $\langle n(t)n(t')\rangle = 2D\delta(t-t')$, Ω is the mean frequency of the resonant drive signal, and $\theta(t)$ is the phase of the drive signal which captures the phase diffusion and frequency fluctuation of the source. We assume that the parametric pump, $4\delta\Gamma\Omega\cos(2\Omega t + 2\theta(t) + \psi)$, is generated by a frequency doubling and a phase shift of the resonant drive, $V_0\cos\big(\Omega t + \theta(t)\big)$ (similarly to our experimental setup). Hence, the pump signal carries the phase, $2\theta(t)$. We assume that the damping, driving, and noise $n(t)$ is weak. The source phase noise, $\theta(t)$, is not assumed to be small, but is assumed to be slow such that $\dot{\theta}$ is small. The resonator frequency fluctuation, $\xi(t)$, is assumed to be weak and slow. We further assume that the mean drive frequency, Ω, is close to the natural frequency such that $\Omega = \omega_0 + \sigma$ where σ, the frequency detuning, is small. Under these conditions the system can be analyzed by perturbation. To facilitate this we first introduce the coordinate transformation,

$$q = u\cos(\Omega t + \theta) + v\sin(\Omega t + \theta), \tag{A2}$$

$$\dot{q} = -\big(\Omega + \dot{\theta}\big)u\sin(\Omega t + \theta) + \big(\Omega + \dot{\theta}\big)v\cos(\Omega t + \theta), \tag{A3}$$

where u and v are the new state variables. Applying equations (A2) and (A3) to equation (A1) gives a system of first order differential equations for u and v in which $\dot{u}$ and $\dot{v}$ are small and cyclo-stationary in time. This makes the systems amenable to the method of averaging [1], [2]. The perturbation analysis results in the set of slow flow equations,

$$\dot{u} \approx -\Gamma(1 + \delta\sin\psi)u + \Gamma\left(\sigma + \delta\cos\psi + \frac{\dot{\theta} - \xi}{\Gamma}\right)v + n_1(t), \tag{A4}$$

$$\dot{v} \approx -\Gamma\left(\sigma - \delta\cos\psi + \frac{\dot{\theta} - \xi}{\Gamma}\right)u - \Gamma(1 - \delta\sin\psi)v - \frac{V_0}{2\Omega} + n_2(t), \tag{A5}$$

where $n_1(t)$ and $n_2(t)$ are two Gaussian white noises with $\langle n_i(t)n_j(t')\rangle \approx \frac{D}{\Omega^2}\delta_{ij}\delta(t-t')$. We assume that all fluctuations in this system have zero mean. Thus, the underlying average flow in equations (A4) and (A5), that is $\langle\dot{u}\rangle$ and $\langle\dot{v}\rangle$, has a fixed point at $(\bar{u}, \bar{v})$ with,

$$\bar{u} = \frac{\sigma + \delta\cos\psi}{\delta^2 - \sigma^2 - 1}\frac{V_0}{2\Gamma\Omega}, \qquad \bar{v} = \frac{1 + \delta\sin\psi}{\delta^2 - \sigma^2 - 1}\frac{V_0}{2\Gamma\Omega}, \tag{A6}$$

The eigenvalues of this fixed point are $\lambda_{\pm} = -\Gamma\left(1 \pm \sqrt{\delta^2 - \sigma^2}\right)$. For $\delta^2 - \sigma^2 < 1$ this fixed point is stable. At $|\delta| = \sqrt{1+\sigma^2}$ the fixed point undergoes a bifurcation and becomes unstable. However, we concern ourselves with the case $|\delta| < \sqrt{1+\sigma^2}$. Provided the fixed point is stable the noise terms in equations (A4) and (A5) will cause the system to fluctuate about this fixed point. We refer to this fluctuation as $\tilde{u} = u - \bar{u}$ and $\tilde{v} = v - \bar{v}$. This fluctuation is assumed to be small and so we disregard the product of $\tilde{u}$ or $\tilde{v}$ with $\dot{\theta}$ or ξ in the equations for $\dot{\tilde{u}}$ and $\dot{\tilde{v}}$ to arrive at

$$\begin{pmatrix}\dot{\tilde{u}}\\ \dot{\tilde{v}}\end{pmatrix} \approx \Gamma \begin{bmatrix}-1-\delta\sin\psi & \sigma+\delta\cos\psi\\ -\sigma+\delta\cos\psi & -1+\delta\sin\psi\end{bmatrix}\begin{pmatrix}\tilde{u}\\ \tilde{v}\end{pmatrix} + \begin{pmatrix}\bar{u}\\ \bar{v}\end{pmatrix}(\dot{\theta}-\xi) + \begin{pmatrix}n_1\\ n_2\end{pmatrix}. \tag{A7}$$

It is interesting to examine the absolute phase of the resonator response,

$$\phi = \theta + \arctan\frac{v}{u}. \tag{A8}$$

For weak noise the fluctuation in the resonator phase is,

$$\tilde{\phi} = \phi - \bar{\phi} \approx \theta + \frac{\bar{u}\tilde{v} - \tilde{u}\bar{v}}{\bar{u}^2 + \bar{v}^2}. \tag{A9}$$

It is straightforward to solve equation (A7) and calculate the power spectrum of $\tilde{\phi}$. The expression, however, is rather cumbersome. We, therefore report the spectrum only for the particular interesting case in which the resonator is driven at resonance and the parametric pump is phase shifted to attenuate the amplitude of oscillation: $\psi = \pi/2$ and $\sigma = 0$. In addition we assume that $\theta(t)$, $\xi(t)$, and $n(t)$are uncorrelated. In this case we have

$$S_{\phi}(\omega) = \frac{\Gamma^2}{\Gamma^2(1+\delta)^2 + \omega^2}\left((1+\delta)^2 S_{\theta}(\omega) + \frac{S_{\xi}(\omega)}{\Gamma^2} + (1-\delta)^2\frac{4D}{V_0^2}\right). \tag{A10}$$

This case is of particular interest because one eigenvector aligns with azimuthal direction in the (u, v) plane. Indeed, for this case the fixed point is $(\bar{u}, \bar{v}) = (0, -V_0/2\Gamma\Omega(1-\delta))$ and the eigenvectors are $\hat{e}_+ = (1,0)$ and $\hat{e}_- = (0,1)$ for $\delta < 0$ or $\hat{e}_+ = (0,1)$ and $\hat{e}_- = (1,0)$ for $\delta > 0$. When the eigenvector is orthogonal to $(\bar{u}, \bar{v})$it is aligned to the azimuth.The slow eigenvector is in the azimuthal direction when $\delta < 0$ and the fast eigenvector is in the azimuthal direction when $\delta > 0$. Note that $\delta > 0$ corresponds to parametric amplification and additional nonlinear terms can become important as the amplitude of oscillation grows. $\delta < 0$ corresponds to parametric attenuation for which the amplitude of oscillation is suppressed and additional nonlinear terms are less likely to become important. By manipulating the parametric pump coefficient, δ, the eigenvalue along the azimuthal direction can be made slower or faster. Now, from equation (A10) we see that the Mathieu resonator becomes

insensitive to the phase noise of the source, S_θ, as $\delta \to -1$.In this limit the resonator close-in phase noise will be dominated by S_ξ/ω^2, which is identical to the phase noise that the frequency fluctuations, $\xi(t)$, would generate if the resonator described by equation (A1) were to be used as the frequency selective element in a closed-loop oscillator. Indeed, if we seek to minimize equation (A10) with respect to δ while ignoring the white noise, *i.e.*let $D \to 0$, we find

$$\frac{\partial S_\phi}{\partial \delta} = \frac{2\Gamma^2(1+\delta)}{(\Gamma^2(1+\delta)^2+\omega^2)^2}\Big(S_\xi(\omega) - \omega^2 S_\theta(\omega)\Big). \tag{A11}$$

Equation (A11) clearly shows that when the frequency fluctuation of the source, $\omega^2 S_\theta = S_{\dot\theta}$, is less than the frequency fluctuation of the Mathieu resonator, S_ξ, then $S_\phi$is reduced by increasing δ. This means approaching the bifurcation point at $\delta \to 1$.On the other hand, when the frequency fluctuations of the source are greater than the frequency fluctuations of the Mathieu resonator, then S_ϕ is reduced by decreasing δ, thereby approaching the bifurcation point at $\delta \to -1$. In this case, $S_\phi$approaches the limit set by the Mathieu resonator. It is important to recall that this model is valid only sufficiently far from the bifurcation point. The model breaks down when the amplitude of oscillation becomes too large or the system is placed sufficiently close to the bifurcation point such that the probability for the noise to push the system out of the domain of attraction becomes significant. Both considerations require the inclusion of nonlinear terms before they can be examined, *c.f.* [3], [4].

The presented theory provides a generalized description of PN shaping of a source undergoing parametric filtering. The agreement between theory and experiment is confirmed by how the PN slope is changing when filtered by a parametric resonator as shown in Fig. A-1. The PN changes its slope from $1/f^3$ (unfiltered case) to $1/f^5$ followed by regions of $1/f^3$ and $1/f^2$.

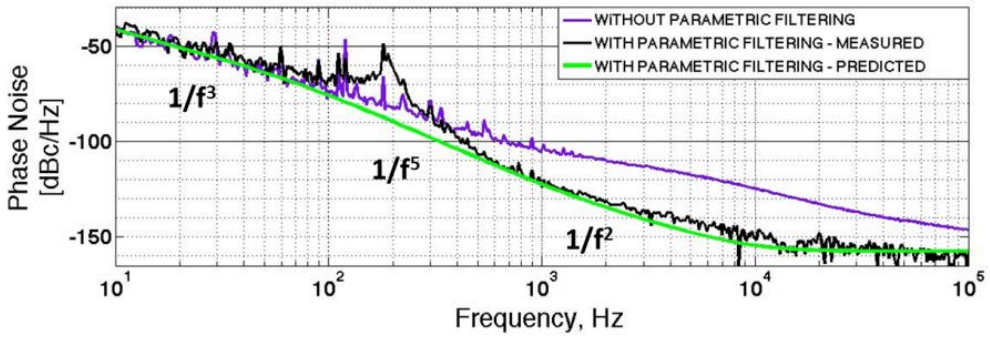

Figure A-1: Effect of Parametric Filtering on the Phase Noise of an External Oscillator
(As described by the theory presented in this section) A clear change in the slope of the PN is observed when filtered by a parametric resonator. The theoretical prediction is in line with our experiments.

6.0 References

[1] Guckenheimer, J., and Holmes, P., “Nonlinear Oscillations, Dynamical Systems, and Bifurcations of Vector Fields”, Applied Mathematical Sciences (Book 42), *Springer*, 2002.

[2] Miller, N.J. “Noise in Nonlinear Micro-Resonators”, Dissertation, Michigan State University, East Lansing, 2012.

[3] Rhoads, J.F., and Shaw, S.W., “The impact of nonlinearity on degenerate parametric amplifiers”, *Applied Physics Letters*, vol. 96, 234101, 2010.

[4] Miller, N.J. “Escape statistics for parameter sweeps through bifurcations”, *Phys. Rev. E.*, vol. 85, 046202, 2012.

7.0 LIST OF PUBLICATIONS

JOURNAL PAPERS

A. Tazzoli, M. Rinaldi, G. Piazza, “Experimental Investigation of Thermally Induced Non-Linearities in Aluminum Nitride Contour Mode MEMS Resonators”, IEEE Electron Device Letters, Vol. 33, Issue 5, 2012, pp. 724-726.

J. S.-Fernandez, G. Piazza, “Thermal Nonlinearities in Contour Mode AlN Resonators”, IEEE Journal of MicroElectroMechanical Systems, 2013, in press.

Z. Yie, M. A. Zielke, C. B. Burgner, and K. L. Turner, “Comparison of Parametric and Linear Mass Detection In the Presence of Detection Noise”, Journal of Micromechanics and Microengineering, vol. 21, 2011.

CONFERENCE PUBLICATIONS

G. Piazza, A. Tazzoli, N. Miller, J. S.-Fernandez, C. Cassella, J. Koo, B. Otis, K. McNaul, B. Gibson, K. Turner, T. Palmer, “Dynamics of Microscale Thin Film AlN Piezoelectric Resonators Enables Low Phase Noise UHF Frequency Sources”, accepted to 2013 IEEE International Frequency Control Symposium.

N. Miller, G. Piazza, “Nonlinear Dynamics in Aluminum Nitride Contour-Mode Resonators”, accepted to 2013 IEEE International Frequency Control Symposium.

N. Miller, G. Piazza, “Vector Network Analyzer Measurements of Frequency Fluctuations in Aluminum Nitride Contour-Mode Resonators”, accepted to 2013 IEEE International Frequency Control Symposium.

C. Cassella, M. Cremonesi, J. S.-Fernandez, A. Frangi, G. Piazza, "Reduction of Anchor Losses by Etched Slots in Aluminum Nitride Contour Mode Resonators", accepted to 2013 IEEE International Frequency Control Symposium.

J. S.-Fernandez, C. Cassella, G. Piazza, “Close-in Phase Noise Reduction in an Oscillator based on 222 MHz Non-Linear Contour Mode AlN Resonators”, accepted to 2013 IEEE International Frequency Control Symposium.

C. Cassella, J. S.-Fernandez, G.Piazza, "Segmented Electrode Excitation of Aluminum Nitride Contour Mode Resonators to Optimize the Device Figure of Merit", accepted for publication in the Proc. of Transducers 2013, June 16-20, 2013, Barcelona, Spain.

J. S.-Fernandez, M. Cremonesi, C. Cassella, A. Frangi, G. Piazza, “Experimental Study on the Impact of Anchor Losses on the Quality Factor of Contour Mode AlN Resonators”, accepted for publication in the Proc. of Transducers 2013, June 16-20, 2013, Barcelona, Spain.

A. Tazzoli, G. Piazza, “Low Power Consumption, Temperature, and Acceleration Insensitive Clocks Based on Ovenized UHF AlN MEMS Resonator”, INVITED paper at 22nd Workshop on Advances in Analog Circuit Design, Grenoble, France, 16-18 April, 2013.

A. Tazzoli, N.-K. Kuo, M. Rinaldi, H. Pak, D. Fry, D. Bail, D. Stevens, Gianluca Piazza, “A 586 MHz Microcontroller Compensated MEMS Oscillator Based on Ovenized Aluminum Nitride Contour-Mode Resonators”, Proceedings of the IEEE International Ultrasonics Symposium (IUS) 2012, Dresden, Germany, 7-10 October 2012, in press.

J. S.-Fernandez, N.-K. Kuo, G. Piazza, “Impact of Metal Electrodes on the Figure of Merit ($k_t^2 \cdot Q$) and Spurious Modes of Contour Mode AlN Resonators”, Proceedings of the IEEE International Ultrasonics Symposium (IUS) 2012, Dresden, Germany, 7-10 October 2012, in press.

A. Tazzoli, M. Rinaldi, G. Piazza, “Ultra High Frequency Temperature Compensated Oscillators Based on Ovenized AlN Contour-Mode MEMS Resonators”, IEEE International Frequency Control Symposium, 21-24 May 2012, Baltimore, MD, in press.

M. Rinaldi, C. Zuniga, A. Tazzoli, G. Piazza, “High Frequency AlN MEMS Resonators with Integrated Nano Hot Plate for Temperature Controlled Operation”, Proc. of IEEE International Frequency Control Symposium 2012, 21-24 May 2012, Baltimore, MD, in press.

M. Rinaldi, A. Tazzoli, C. Zuniga, G. Piazza, “A 970 MHz Ovenized Oscillator based on an AlN MEMS Resonator with monolithically Integrated Suspended Nano Hot Plate”, Hilton Head Workshop, 3-7 June, 2012.

A. Tazzoli, G. Piazza, M. Rinaldi, J. Segovia, C. Cassella, B. Otis, J. Shi, K. Turner, C. Burgner, K. McNaul, D. Bail, V. Felmetsger, “Piezoelectric Non-Linear Nanomechanical Temperature and Acceleration Insensitive Clocks”, INVITED paper at SPIE, Baltimore 2012, Proc. SPIE 8373, Micro- and Nanotechnology Sensors, Systems, and Applications IV, 83730A (May 1, 2012); doi:10.1117/12.920845.

M. Rinaldi, A. Tazzoli, J. Segovia-Fernandez, V. Felmetsger, G. Piazza, “High Power and Low Temperature Coefficient of Frequency Oscillator Based on a Fully Anchored and Oxide Compensated AlN Contour-Mode Mems Resonator”, Proc. of MEMS 2012, Paris, France, Jan. 29 - Feb. 2, 2012, pp. 696 - 699.

A. Tazzoli, M. Rinaldi, G. Piazza, “Ovenized High Frequency Oscillators Based on Aluminum Nitride Contour Mode MEMS Resonators”, Proc. of IEDM 2011, Washington, D.C., 5-7 Dec. 2011, pp. 20.2.1 - 20.2.4.

A. Tazzoli, M. Rinaldi, C. Zuo, N. Sinha, J. V. der Spiegel, G. Piazza, “Aluminum Nitride Reconfigurable RF-MEMS Front-Ends”, INVITED paper at ASICON 2011, Xiamen, China, 25-28 Oct. 2011, pp. 1046 - 1049.

J. S.-Fernandez, A. Tazzoli, M. Rinaldi, G. Piazza, “Nonlinear lumped electrical model for Contour Mode AlN Resonators”, Proc. of IEEE International Ultrasonics Symposium 2011, Orlando, FL, 18-21 Oct. 2011, pp. 1846 - 1849.

C. B. Burgner, L. A. Shaw, and K. L. Turner, “A New Method For Resonant Sensing Based on Noise In Nonlinear Mems”, in 2012 IEEE 25th International Conference on Micro Electro Mechanical Systems, 2012.

C. B. Burgner, W. S. Snyders, and K. L. Turner, “Control of Mems on the Edge of Instability”, in Transducers 2011 - 2011 16th International Solid-state Sensors, Actuators and Microsystems Conference, 2011.

K.L.Turner, C.B. Burgner, Z. Yie, E. Holtoff “Using nonlinearity to enhance micro/nanosensor performance”, INVITED paper at IEEE Sensors, 2012, 28-31 Oct. 2012, p. 1-4

List of Acronyms, Abbreviations, and Symbols

ACRONYM	DESCRIPTION
ADS	advanced design system
AlN	aluminum nitride
CMR	contour-mode resonator
dBc	decibel
DC	direct current
GHz	gigahertz
Hz	hertz
IC	integrated circuit
IME	Institute of Microelectronics
kHz	kilohertz
LC	lumped component
MEMS	micro-electrical mechanical system
MHz	megahertz
PENNTAC	Piezoelectric Non-Linear Nanomechanical Temperature and Acceleration Intensive Clocks
PCB	printed circuit board
PN	phase noise
RF	radio frequency
SMA	subminiature version A
SNL	Sandia National Laboratories
TCF	temperature coefficient of frequency